Sex-specific post-translational regulation of the gamete fusogen GCS1 in the isogamous volvocine alga Gonium pectorale

Hiroko Kawai-Toyooka, Toshiyuki Mori, Takashi Hamaji, Masahiro Suzuki, Bradley J. S. C. Olson, Tomohiro Uemura, Takashi Ueda, Akihiko Nakano, Atsushi Toyoda, Asao Fujiyama, and Hisayoshi Nozaki

Published Version Information

Citation: Kawai-Toyooka, H., Mori, T., Hamaji, T., Suzuki, M., Olson, B. J. S. C., Uemura, T., Ueda, T., Nakano, A., Toyoda, A., Fujiyama, A., & Nozaki, H. (2014). Sex-specific posttranslational regulation of the gamete fusogen GCS1 in the isogamous volvocine alga Gonium pectoral. Eukaryotic Cell, 13(5), 648-656.

Digital Object Identifier (DOI): doi:10.1128/EC.00330-13

Publisher's Link: http://ec.asm.org/content/13/5/648

Sex-specific Post-translational Regulation of the Gamete Fusogen GCS1 in the Isogamous Volvocine Alga *Gonium pectorale*

Hiroko Kawai-Toyooka,[a] Toshiyuki Mori,[b] Takashi Hamaji,[c] Masahiro Suzuki,[a] Bradley J.S.C. Olson,[d] Tomohiro Uemura,[a] Takashi Ueda,[a] Akihiko Nakano,[a,e] Atsushi Toyoda,[f] Asao Fujiyama,[f] and Hisayoshi Nozaki[a]#

Department of Biological Sciences, Graduate School of Science, University of Tokyo, Tokyo, Japan[a]; Waseda Institute for Advanced Study, Waseda University, Tokyo, Japan[b]; Department of Botany, Graduate School of Science, Kyoto University, Kyoto, Japan[c]; Ecological Genomics Institute, The Division of Biology, Kansas State University, Manhattan, Kansas, USA[d]; Live Cell Molecular Imaging Research Team, RIKEN Center for Advanced Photonics, Saitama, Japan[e]; Comparative Genomics Laboratory, National Institute of Genetics, Shizuoka, Japan[f]

Running Head: Sex-specific regulation for gamete fusogen

#Address correspondence to Hisayoshi Nozaki, nozaki@biol.s.u-tokyo.ac.jp.

ABSTRACT

Male and female, generally defined based on differences in gamete size and motility, likely have multiple independent origins, appearing to have evolved from isogamous organisms in various eukaryotic lineages. Recent studies of the gamete fusogen GCS1/HAP2 indicate that this protein is deeply conserved across eukaryotes, and its exclusive and/or functional expression generally resides in males or in male homologues. However, little is known regarding the conserved or primitive molecular traits of males and females within eukaryotes. Here, using morphologically indistinguishable isogametes of the colonial volvocine *Gonium pectorale*, we demonstrated that GCS1 is differently regulated between the sexes. *G. pectorale* GCS1 molecules in one sex (homologous to "male") are transported from the gamete cytoplasm to the protruded fusion site, whereas those of the other sex ("females") are quickly degraded within the cytoplasm upon gamete activation. This molecular trait difference might be conserved across various eukaryotic lineages and may represent male and female prototypes originating from a common eukaryotic ancestor.

INTRODUCTION

Sex might have first evolved in the common ancestor of all eukaryotes ~2 billion years ago because sex and sex-related genes are widespread within the eukaryotes (1). However, little is known about sex in the ancient common eukaryotic ancestor. “Isogamy” is primitive sexual reproduction involving gametes of identical size and motility. “Oogamy” appears to have evolved from isogamy in nearly all lineages of multicellular organisms (2), and manifests as small motile gametes (sperm) in “males” and large immotile gametes (eggs) in “females” (3). Therefore, sexual dimorphism in male and female gametes and sex-specific gamete-interaction factors likely result from parallel and multiple evolutions. However, recent studies of GENERATIVE CELL SPECIFIC 1/HAPLESS 2 (GCS1/HAP2) suggest that a common mechanism for gamete fusion could exist across various eukaryotic lineages (4). GCS1/HAP2 is a gamete-specific transmembrane protein that is essential for fertilization and is widely conserved in diverse eukaryotic lineages, indicating that *GCS1/HAP2* is likely to have been present in the common ancestor of eukaryotes (4). Although *GCS1/HAP2* genes are present in the nuclear genome of both sexes, exclusive and/or functional *GCS1/HAP2* expression generally resides in the male or male homologue in flowering plants, green algae, malaria parasites, and metazoan species (5–8). Since various separate lineages of sexually reproducing eukaryotes lack *GCS1/HAP2* in their genomes, this gene seems to have been lost and alternative male gamete fusogens, such as the immunoglobulin superfamily protein IZUMO1 in mammalians (9), are considered to have evolved to replace the function of GCS1/HAP2 in these organisms (4).

Functional studies of *GCS1/HAP2* have been based on oogamous organisms in which fundamental differences in molecular mechanisms of GCS1/HAP2 between the sexes appear ambiguous due to the differences in size and motility between egg and sperm (5, 8), or on the unicellular volvocine alga *Chlamydomonas reinhardtii*, which produces morphologically

distinct mating type *plus* and *minus* isogametes (7). Interestingly, *GCS1/HAP2* expression in *C. reinhardtii* is not exclusive to *minus* gametes; slight up-regulation of *GCS1/HAP2* is also detected in *plus* after gamete differentiation (5), although the *plus GCS1/HAP2* expression is not functional (7). However, details of sex-specific regulation of this gene remain unresolved.

To explore the dynamics of GCS1, we focused on the morphologically indistinguishable *plus* and *minus* isogametes in the colonial volvocine alga *Gonium pectorale*. The isogamous system in *G. pectorale* offers a model system for focusing on the mating-type specificity of GCS1 (Fig. 1). In *C. reinhardtii*, *plus* gametes bear a ~3-μm-long "tubular mating structure (TMS)" or "fertilization tubule" filled with actin filaments, whereas the mating structure of *minus* gametes is dome-shaped without actin accumulation (10–13). GCS1/HAP2 in *C. reinhardtii* is localized at the *minus* mating structure and mediates membrane fusion with *plus* gametes (7). In contrast, *plus* and *minus* gametes in *G. pectorale* are morphologically identical, bearing TMS (bilateral TMS, 14,15; Fig. 1A). We recently established a novel experimental system for examining the activated, TMS-bearing *G. pectorale* gametes induced in each sex (15) (Fig. 1B). Moreover, in volvocine algae, mating type *minus* in isogamous species is homologous to male in anisogamous/oogamous species, based on the presence of the sex-determining *minus*-dominance (*MID*) genes in male genomes (16–20) (Fig. 1A). Therefore, the simple isogamous system in *G. pectorale* enables us to dissect fundamental differences in GCS1 behavior between the sexes in association with the male-female dichotomy.

In this study, we identified a full-length *G. pectorale GCS1* (*GpGCS1*) coding sequence from our ongoing nuclear genome project. Using an antibody against the GpGCS1 protein, we precisely analyzed the expression and localization pattern of the protein and discovered that sex-specific, stepwise regulation localizes GpGCS1 at the surface of the TMS in a *minus*-specific manner. These regulatory mechanisms are considered to be the biological

basis for the sex-specific action of GCS1/HAP2 at the cellular level, and may be conserved among various eukaryotic lineages.

MATERIALS AND METHODS

***Gonium* strains, culture conditions, and gamete induction.** Strains K41 (mating-type *plus*) and K34 (mating-type *minus*) of *Gonium pectorale* (15) were used for the analyses of the *GpGCS1* gene expression and the experiments with the anti-GpGCS1 antibody. For identification of the *GpGCS1* gene, another *minus* strain (K3-F3-4; 21) was used. In order to strengthen the sex-dependent expression of *GpGCS1*, we also examined four wild strains: two parental strains of K41 and K34, Kaneko4 (mating-type *plus*) and Kaneko3 (mating-type *minus*)(15), and two other strains of *G. pectorale* (originating from the same soil sample as Kaneko4 and Kaneko3; 22), Kaneko8 (mating-type *plus*) and Kaneko2 (mating-type *minus*). Culture conditions were described previously (21) with continuous aeration. Vegetative cells were harvested from 3-day-old cultures. To obtain gametes, 10–15 ml of a 3- to 4-week-old culture of each strain (~6×10^6 cells) were concentrated to 1.0–1.5 ml by centrifugation, transferred to a 3.5-cm petri dish and cultured at 25ºC for 3–5 h. For gamete activation, cells were treated for 1–3 h with 15 mM db-cAMP (dibutyryl cyclic adenosine monophosphate) and 1 mM IBMX (3-isobutyl-1-methylxanthine), as described previously (15).

Identification of the *GpGCS1* gene. We performed a BLAST search against the preliminary genome assembly database of *G. pectorale minus* strain (K3-F3-4), with *Chlamydomonas reinhardtii* GCS1/HAP2 (accession number: EF397563) as the query, and retrieved several sequences with significant homology; we based the design of *GpGCS1*-specific primers on these sequences. To identify the cDNA sequence of *GpGCS1,* polyadenylated mRNAs from *minus* (K3-F3-4) gametes were isolated using Dynabeads Oligo $(dT)_{25}$ (Life Technologies, Carlsbad, CA), reverse-transcribed with Superscript III reverse transcriptase (Life Technologies), and amplified with KOD FX Neo DNA polymerase (Toyobo, Osaka, Japan) and the *GpGCS1*-specific primers. We performed rapid amplification of 3'-cDNA ends (3′

RACE) using the GeneRacer kit (Life Technologies). The PCR products were directly sequenced using an ABI PRISM 3100 Genetic Analyzer (Life Technologies) using BigDye Terminator Cycle Sequencing Ready Reaction Kit v. 3.1 (Life Technologies). To determine the genomic sequence, a bacterial artificial chromosome (BAC) clone covering the *GpGCS1* locus from *G. pectorale* Kaneko3 (clone 016G17; available from Clemson University Genome Institute [CUGI], Clemson, SC) was subjected to shotgun sequencing using ABI 3730xl capillary DNA sequencers (Life Technologies). The cDNA sequence from the K3-F3-4 gametes was confirmed to be completely identical with the exon sequence obtained from the BAC clone sequencing. The cDNA and genomic sequence of *GpGCS1* have been deposited in the DDBJ database under accession numbers AB915401 and AB915402, respectively.

Amino acid sequence alignment and domain predictions. Alignment of deduced amino acid sequences of *G. pectorale* and *C. reinhardtii* GCS1/HAP2 was constructed using MUSCLE (http://www.ebi.ac.uk/Tools/msa/muscle/) and shaded by BOXSHADE 3.21 (http://www.ch.embnet.org/software/BOX_form.html). Identity between GpGCS1 and CrGCS1/HAP2 was calculated from pairwise distances computed by MEGA5 (23). All positions containing gaps and missing data were eliminated. Signal sequences, HAP2-GCS1, and transmembrane domains were predicted using SignalP 4.0 (http://www.cbs.dtu.dk/services/SignalP-4.0/), Pfam 26.0 (http://pfam.janelia.org/search), and Phobius (http://phobius.sbc.su.se/), respectively. Putative N-glycosylation sites were predicted by NetNGlyc 1.0 (http://www.cbs.dtu.dk/services/NetNGlyc/) with a potential score >0.5.

Phylogenetic analysis of GCS1/HAP2. For GCS1/HAP2 phylogeny, deduced amino acid sequences of *GpGCS1* and *GCS1* homologs of *Volvox carteri* (XP_002952884.1 [hypothetical protein VOLCADRAFT_10570] and XP_002952883.1 [hypothetical protein VOLCADRAFT_105707]) and *Coccomyxa subellipsoidea* (EIE26501.1 [hypothetical protein COCSUDRAFT_39583]) were aligned with the data matrix of (7) by using a BLASTP search of NCBI (http://www.ncbi.nlm.nih.gov/) and Clustal X (24). After removing a previously included *Volvox carteri* GCS1 homolog, short sequences, and long-branched amitochondrial excavates, a data matrix of 239 amino acid positions from 29 operational taxonomic units was analyzed. The amino acid alignment of GCS1/HAP2 proteins has been deposited in TreeBASE under accession number S15345 (http://www.treebase.org/treebase-web/home.html). Phylogenetic analyses were performed under maximum likelihood (ML) using RAxML (25) (with WAG+I+4G model) and PhyML 3.0 (26) (with LG+I+4G model) with 100 bootstrap replicates.

Semi-quantitative reverse-transcribed (RT)-PCR analysis. Polyadenylated mRNA from each sample was isolated, reverse-transcribed, and subjected to PCR analysis as described above, using *GpGCS1*-specific primers (5′-GTGCATCGCCGACGGGGTTACCGA-3′ and 5′-CAGCGGCGACTTGGTCAGCGACAC-3′) and KOD FX Neo DNA polymerase (Toyobo). The PCR schedule was 2 min at 94ºC followed by 30 cycles of 10 s at 98ºC, and 30 s at 68ºC. The resultant 232-bp fragments were directly sequenced for confirmation. *EF-like* and *GpMID* genes were amplified using previously described primer sets (CV_EF1A1-R2 and GpEF1A-INT3-R for *EF-like*; GPMID_int1F and GPMID_int4R for *GpMID*) (18) and KOD-plus-Neo DNA polymerase (Toyobo). The PCR schedule was 2 min at 94ºC followed by 25 cycles of 10 s at 98ºC, 30 s at 63ºC, and 40 s at 68ºC. The amplified products were electrophoresed on 2% (w/v) agarose gels and stained with ethidium bromide. The gel

images were captured using a ChemiDoc XRS system with the Quantity One software (Bio-Rad, Hercules, CA) and level-adjusted with Adobe Photoshop CS6 (Adobe Systems Inc., San Jose, CA).

Antibody production. The 5′ region of the *GpGCS1* cDNA sequence (1,738 bp) was amplified using high-fidelity KOD-Plus-DNA polymerase (Toyobo) and *GpGCS1* specific primers (5′-ATAGCACGCCGCGAAGCGACACTC-3′, 5′-CGGCGTCGTACAGCGTCAGCCAAC-3′), and cloned into pCR4Blunt-TOPO vector (Life Technologies). The *Bgl*II–*Sph*I fragment (corresponding to amino acid residues 28–356) of the insert was cloned into the expression vector pQE-82L (Qiagen, Hilden, Germany) and transformed into *Escherichia coli* Rosetta competent cells (Merck Millipore, Billerica, MA) to prepare recombinant partial GpGCS1 protein. The recombinant proteins were extracted from bacterial cells using an xTractor buffer kit (Clontech, Mountain View, CA), and purified using a HisTrap HP column with a His buffer kit (GE Healthcare, Uppsala, Sweden) according to the manufacturers' instructions. The purified protein was subjected to sodium dodecyl sulfate-polyacrylamide gel electrophoresis (SDS-PAGE) and gel slices containing the ~30-kDa recombinant protein were injected into a rabbit to obtain polyclonal antiserum (TK Craft, Gunma, Japan). From the antiserum, IgG was purified using a MAbTrap kit (GE Healthcare) and used as an anti-GpGCS1 antibody.

Immunoblotting analysis. Cells from each condition were harvested by centrifugation, resuspended in sodium dodecyl sulfate (SDS) sample buffer (50 mM Tris-HCl [pH 6.8], 2% SDS, 10% glycerol, 100 mM DTT, 1 mM PMSF, 1% protease inhibitor cocktail [P9599, Sigma-Aldrich, St. Louis, MO], Complete protease inhibitor cocktail tablets [Roche Diagnostics, Mannheim, Germany] and 0.02% bromophenol blue) and incubated at 70ºC for

10 min. After centrifugation, the supernatants were loaded and separated on a 7.5% Mini-PROTEAN TGX precast gel (Bio-Rad) and blotted onto a Hybond-P membrane (GE Healthcare). The blot was blocked with Blocking One (Nacalai Tesque, Kyoto, Japan) at 4ºC, and incubated overnight with the anti-GpGCS1 antibody (1:5000 dilution) at 4ºC. The blots were then incubated with an anti-IgG antibody conjugated to horseradish peroxidase (1:100000 dilution, Jackson ImmunoResearch, West Grove, PA) and protein bands were detected with Amersham ECL Prime Western blotting detection reagent (GE Healthcare). For Coomassie Brilliant Blue (CBB)-staining, SDS-PAGE gels were stained with EzStain AQua (ATTO, Tokyo, Japan). Images were recorded using a ChemiDoc XRS system with the Quantity One software and level-adjusted with Adobe Photoshop CS6.

Light microscopy. Light microscopy was performed using a BX61 microscope (Olympus, Tokyo, Japan) equipped with differential interference contrast optics and a BX60 microscope (Olympus) equipped with phase-contrast optics. The images were level-adjusted with Adobe Photoshop CS6.

Indirect immunofluorescence analysis. Immunostaining was performed as described previously (27) with modification. In brief, gametes were attached to coverslips precoated with 0.1% polyethylenimine, fixed by 3.7% formaldehyde-containing solution, and extracted by detergent to remove chlorophyll autofluorescence. After washing and blocking steps, the cells were incubated overnight with the GpGCS1 antibody (1:1000 dilution) and/or an anti-actin antibody (1:2000 dilution; clone C4, MP Biomedicals, Morgan, CA) at 4ºC. The cells were again washed, blocked, and stained with Alexa Fluor 488 goat anti-rabbit and/or 568 goat anti-mouse IgG (1:1000 dilution each; Life Technologies) for 1–3 h at room temperature. The cells were then washed and mounted with ProLong Gold or *SlowFade* Gold

Antifade reagents (Life Technologies). For activated gametes without cell walls, the chlorophyll extraction step and all detergents in the solutions were omitted because they tended to cause bursting of the cells. For unactivated gametes, images were captured using an LSM780 confocal microscope (Carl Zeiss, Oberkochen, Germany) with an oil-immersion lens (X63, NA = 1.40) and ZEN 2011 software (Carl Zeiss). For activated gametes, images were captured using a BX60 microscope with an UPlanFLN 100X/1.3 objective (Olympus). The Adobe Photoshop CS6 software was used for level-adjustment and preparation of merged images.

RESULTS

Identification and characterization of *GpGCS1*. We performed a BLAST search against the *G. pectorale* genome assembly with *C. reinhardtii GCS1/HAP2* (*CrGCS1/HAP2*) as a query, and found one locus with significant similarity. Based on RT-PCR, genomic PCR, and 3′RACE analysis, we identified a full-length coding sequence (3,408 bp) and exon-intron structure of the *G. pectorale GCS1* (*GpGCS1*) gene. The *GpGCS1* gene comprises 13 exons, and three polyadenylation sites are found in the 3′-untranslated region (Fig. 2A). The GC content of the *GpGCS1* coding sequence was high (72.6%), similar to that of *CrGCS1/HAP2* (69.4%). Alignment of deduced amino acid sequences of GCS1/HAP2 from *G. pectorale* and *C. reinhardtii* revealed that the N-terminal halves of the two proteins had particularly high similarity (Fig. 2B). The total identity between the two sequences was 60.3%. Putative signal sequence and transmembrane domains were conserved in both sequences, suggesting that these proteins are targeted to the plasma membrane. The HAP2-GCS1 domain that is highly conserved among the GCS1/HAP2 orthologs was also found with the invariant conservation of cysteine residues, which are predicted to participate in disulfide bonding in an extracellular environment. Liu et al. (28) reported that CrGCS1/HAP2 contains nine putative N-glycosylation sites and showed that the protein is actually N-glycosylated. We compared locations of putative N-glycosylation sites between *C. reinhardtii* and *G. pectorale* GCS1/HAP2 and revealed that five of eight potential N-glycosylation sites in GpGCS1 were conserved in CrGCS1/HAP2. All of these sites were N-terminal to the transmembrane domain, suggesting that sugar chains of volvocine GCS1/HAP2 are exposed to extracellular environments. Additionally, the GCS1/HAP2 proteins from these volvocine algae possessed longer sequences (1,136 amino acids in *G. pectorale* and 1,139 amino acids in *C. reinhardtii*) compared to those from land plants and malaria parasites (e.g., 705 and 828 amino acids in *Arabidopsis thaliana* and *Plasmodium berghei*, respectively), because of the long, single

amino acid repeat-containing sequences that were C-terminal to the transmembrane domain (Fig. 2B). For phylogenetic analysis, two loci found in the *Volvox carteri* genome database version 2.0 (http://phytozome.net/volvox) with significant similarity to *CrGCS1/HAP2* (locus names: Vocar20011213m.g [*V. carteri* 1] and Vocar20000015m.g [*V. carteri* 2]) (Fig. 3) were included. The phylogenetic analysis showed that the GCS1/HAP2 proteins of volvocine algae (*C. reinhardtii*, *G. pectorale*, and *V. carteri*) form a robust monophyletic group (Fig. 3). These results indicated that the structural features of the GCS1/HAP2 proteins are also conserved in GpGCS1 and that the volvocine GCS1 proteins may function by a common mechanism to mediate gamete membrane fusion. Two amoebozoans, *Dictyostelium discoideum* and *Physarum polycephalum*, were unexpectedly positioned in separate lineages in the GCS1/HAP2 tree (Fig. 3). This may represent different patterns of gene evolution in these species. Some of other relationships between major groups of eukaryotes seem to be not well supported, possibly due to the limited information of the amino acid sequences used for the phylogenetic analysis.

Gamete-specific expression of GpGCS1. We performed semi-quantitative RT-PCR analysis using the *GpGCS1*-specific primers (indicated in Fig. 2A) to determine the expression pattern of the *GpGCS1* transcripts. No obvious *GpGCS1* expression was detected in vegetative cells of either sex (Fig. 4; see Fig. S1 in supplemental material). After gamete induction by long-term cultivation (Fig. 1B), *GpGCS1* expression was up-regulated in both sexes, although the up-regulation was more pronounced in *minus* than in *plus* gametes (Fig. 4; see Fig. S1 in supplemental material) and decreased after mixing of the gametes (Fig. 4), as was also seen in *CrGCS1/HAP2* (5). Interestingly, the expression was enhanced in *minus* gametes after activation of the gametes by treatment with db-cAMP and IBMX (Fig. 1B), while *GpGCS1*

expression almost disappeared in *plus* gametes (Fig. 4). Similar enhanced expression was also recognized in *GpMID* of *minus* gametes as reported previously (15) (Fig. 4).

***Minus*-enhanced expression and *plus*-specific degradation of GpGCS1.** To analyze GpGCS1 expression at the protein level, we prepared an antibody against the N-terminal region of GpGCS1 (Fig. 2B). By immunoblotting analysis using the anti-GpGCS1 antibody, the GpGCS1 signal was detected as a major band at ~140 kDa in *plus* and *minus* gametes, whereas no such signal was observed in vegetative cells (Fig. 5A). The quantity of the protein was substantially greater in *minus* than in *plus* gametes, consistent with the results of RT-PCR (Fig. 4). We next examined GpGCS1 dynamics upon gamete activation. In *plus* gametes, the quantity of GpGCS1 protein decreased rapidly and almost disappeared after incubation with db-cAMP and IBMX for 1 h, whereas it remained intact in *minus* gametes (Fig. 5B). This result suggests that gamete activation not only represses *GpGCS1* transcription but also degrades the GpGCS1 protein in a *plus*-specific manner.

***Minus*-specific TMS localization of GpGCS1.** We next performed indirect immunofluorescence analysis using the same antibody to investigate the subcellular localization of GpGCS1. In the unactivated *minus* gamete, a strong GpGCS1 signal was observed at the anterior end of the cell (arrowheads in left panels of Fig. 6A), which is the primordial site for TMS formation in *G. pectorale* (15). Many small punctate signals of GpGCS1 were also observed in the cytoplasm immediately beneath the anterior end, indicating that GpGCS1 is likely to be transported to the primordial TMS site by a significant number of membrane vesicles. In the unactivated *plus* gamete; however, no signal was detected in the anterior end, while punctate signals were observed in the cytoplasm surrounding the nucleus (Fig. 6A, right panels), suggesting that GpGCS1 in *plus* gametes was

not transported to the primordial TMS but instead remained internal. When the gametes were activated, the GpGCS1 signal was observed along the TMS in *minus* but not in *plus* gametes, while accumulation of actin in the TMS was observed in both gametes (15) (Fig. 6B). No obvious GpGCS1 signal was observed in the activated *plus* gamete, which is consistent with the *plus*-specific loss of the GpGCS1 protein revealed by the immunoblotting analysis (Fig. 5B). In the activated *minus* gamete, the GpGCS1 signal was observed along the periphery of the actin filaments and was most concentrated at the tip of the TMS (Fig. 6B, left panels), suggesting that GpGCS1 is localized to the plasma membrane of the *minus* TMS, especially the TMS tip where the *minus* TMS first attaches to the *plus* TMS and membrane fusion appears to be initiated (14).

DISCUSSION

In this study, we identified the GCS1 ortholog from the colonial volvocine alga *G. pectorale,* generated antibody against the GpGCS1 protein, and used this antibody to explore fundamental differences in GCS1 dynamics between two opposite sexes. In *C. reinhardtii*, a unicellular relative of *G. pectorale*, up-regulation of *GCS1/HAP2* gene expression by gamete induction was observed in both sexes (5), but sex-based differences in GCS1 behavior at the protein level were not confirmed. Liu et al. (7, 28) reported that the HA-tagged version of CrHAP2/GCS1 in transgenic *CrGCS1/HAP2-HA minus* strain (*hap2* mutant with introduced *HAP2-HA*) is expressed exclusively in gametes as two differently N-glycosylated isoforms of ~150 and ~140 kDa, the former present on the cell surface and the latter remaining intracellular. Although Liu et al. (28) also reported that CrGCS1/HAP2-HA in *minus* gametes is rapidly degraded after the membrane-fusion event with *plus* gametes as prevention against polygamy, information regarding the GCS1/HAP2 protein in *plus* gametes prior to fusion has been lacking to date. In our immunoblotting experiments with GpGCS1 in *G. pectorale*, only one band was observed to be comparable in size to the lower form of CrGCS1/HAP2-HA (Fig. 5). Given that the putative N-glycosylation sites of GpGCS1 and CrGCS1/HAP2 are not completely conserved (Fig. 2B), the difference in the migration patterns observed between *G. pectorale* and *C. reinhardtii* GCS1/HAP2 may be derived from different glycosylation patterns between the species. Our comparison of the GCS1/HAP2 sequence in *G. pectorale* and *C. reinhardtii* (Fig. 2B) will also provide useful information for identifying actual N-glycosylation sites, their functions, and other functional domains of GCS1 for future study.

By combining the results of our expression and localization analyses, we propose a stepwise regulation model for *minus*-specific GpGCS1 localization on the TMS (Fig. 7). Transcription of *GpGCS1* is inhibited during the vegetative stage in both sexes. After culturing for several weeks to induce starvation, the cells differentiate into gametes and

GpGCS1 transcription is switched on (Fig. 4). *GpGCS1* transcription is specifically up-regulated in the *minus* gametes, resulting in enhanced accumulation of GpGCS1 protein in these gametes (Fig. 5A) (Step 1). However, GpGCS1 protein is also expressed at a substantial level in *plus* gametes (Fig. 5A). After translation, a possible transportation mechanism present only in *minus* gametes enables GpGCS1 to accumulate at the primordial sites for the TMS, whereas GpGCS1 remains within the cytoplasmic region in *plus* gametes (Fig. 6A) (Step 2). After activation of the *plus* and *minus* gametes, intracellular cAMP rapidly increases to trigger cell wall loss and formation of the TMS in both gametes (15). GpGCS1 at the primordial TMS site in *minus* gametes is transported to the plasma membrane of the active TMS (Fig. 6B). In contrast, GpGCS1 distributed in the cytoplasmic region of *plus* gametes rapidly degrades upon gamete activation (Fig. 5B) (Step 3). These regulatory mechanisms are likely to enable GpGCS1 to be specifically localized at the *minus* TMS, and therefore to function as a *minus*-specific fusogen in this organism.

Our immunostaining clearly showed that GpGCS1 was distributed differently in unactivated gametes, in the internal cytoplasm region in *plus* gametes and the anterior primordial TMS site in *minus* gametes (Fig. 6A). This distributional difference between the sexes presumably serves as a cellular basis for the *minus*-specific TMS localization and could be determined by the presence or absence of the *MID* gene, the master regulator for sex determination (16,18). Since the MID protein is thought to be a transcription factor (16), MID may regulate the expression of the component(s) for (i) membrane trafficking machinery that delivers GCS1 to the primordial TMS, or (ii) post-translational modification (such as N-glycosylation) for distinguishing *plus* and *minus* GCS1 molecules to achieve the selective transport of this molecule.

We also showed that the gamete-activation signal induced selective degradation of GpGCS1 in *plus* gametes (Fig. 5B). This selective degradation may be induced by *plus*-

specific signaling, while the *MID* gene negatively regulates this signaling in *minus* gametes. Another potential explanation is that the gamete-activation signal initiates the protein-degradation machinery in the cytoplasm of both *plus* and *minus* gametes, but that rapid translocation of GpGCS1 to the fusion site occurs in *minus* gametes, thus separating the protein from the degradation machinery and allowing it to persist and function in these gametes. The degradation of GpGCS1 may involve proteolytic mechanisms such as autophagy and proteasome-dependent pathways. Further cell biological and biochemical analyses will be necessary to assess these possibilities.

In flowering plants, GCS1/HAP2 was detected as a punctate structure in sperm cells, and redistributed to the cell surface in response to egg cell-secreted EGG CELL 1 protein (29). In *G. pectorale*, punctuated GpGCS1 signals are also observed in the cytoplasm of unactivated gametes of both sexes (Fig. 6A), but the elevation of intracellular cAMP (15) may trigger transport of GCS1 to the fusion site only in *minus* gametes. Such a transportation mechanism for GCS1 might be conserved in males or male homologues across various eukaryotic lineages (5–8), originating from a possible isogamous common ancestor (1, 4). Our findings provide novel molecular insights into the prototypes of male and female prior to evolution of gamete size and motility, although more information from other isogamous organisms is still needed. The opposite sexes in the common ancestor of eukaryotes might have differed from one another in molecular traits of the fusogen GCS1, as resolved in the present study (Fig. 7). Furthermore, multiple or independent evolution of oogamy from isogamy within the eukaryotes (2) might have been based on such sex-dependent differences in GCS1.

The anisogamous/oogamous colonial volvocine algae may have evolved from an ancestral isogamous colonial alga with a bilateral TMS (30, 31) (Fig. 1A). The present molecular biological results for *G. pectorale* provide a promising platform for investigating

how GCS1 dynamics evolved in each sex in association with the isogamy-oogamy transition. Further analyses using the anisogamous and oogamous volvocine algae will help to answer this interesting question of evolutionary biology.

ACKNOWLEDGMENTS

We thank Dr. Yuko Mogi for sharing valuable information and Dr. Patrick J. Ferris for providing useful comments on an early version of the manuscript.

This work was supported by Grants-in-Aid for Scientific Research on Innovative Areas “Genome Science” (grant number 221S0002), JSPS Fellows (grant number 22-40216 to HK-T), Research Activity start-up (grant number 25891009 to HK-T), Challenging Exploratory Research (grant number 24657045 to HN), and Scientific Research (A) (grant number 24247042 to HN) from MEXT/JSPS KAKENHI.

REFERENCES

1. **Zimmer C.** 2009. On the origin of sexual reproduction. Science **324:**1254-1256.
2. **Kirk DL.** 2006. Oogamy: inventing the sexes. Curr. Biol. **16:**R1028-R1030.
3. **Bell G.** 1978. The evolution of anisogamy. J. Theor. Biol. **73:**247-270.
4. **Wong JL, Johnson MA.** 2010. Is HAP2-GCS1 an ancestral gamete fusogen? Trends Cell Biol. **20:**134-141.
5. **Mori T, Kuroiwa H, Higashiyama T, Kuroiwa T.** 2006. GENERATIVE CELL SPECIFIC 1 is essential for angiosperm fertilization. Nat. Cell Biol. **8:**64-71.
6. **Hirai M, Arai M, Mori T, Miyagishima SY, Kawai S, Kita K, Kuroiwa T, Terenius O, Matsuoka H.** 2008. Male fertility of malaria parasites is determined by GCS1, a plant-type reproduction factor. Curr. Biol. **18:**607-613.
7. **Liu Y, Tewari R, Ning J, Blagborough AM, Garbom S, Pei J, Grishin NV, Steele RE, Sinden RE, Snell WJ, Billker O**. 2008. The conserved plant sterility gene *HAP2* functions after attachment of fusogenic membranes in *Chlamydomonas* and *Plasmodium* gametes. Genes Dev. **22:**1051-1068.
8. **Steele RE, Dana CE. 2009.** Evolutionary history of the HAP2/GCS1 gene and sexual reproduction in metazoans. PLoS ONE 4:e7680. doi:10.1371/journal.pone.0007680.
9. **Inoue N, Ikawa M, Isotani A, Okabe M**. 2005. The immunoglobulin superfamily protein Izumo is required for sperm to fuse with eggs. Nature **434:**234-238.
10. **Friedmann I, Colwin AL, Colwin LH.** 1968. Fine-structural aspects of fertilization in *Chlamydomonas reinhardi.* J. Cell Sci. **3:**115–128.
11. **Goodenough UW, Detmers PA, Hwang C.** 1982. Activation for cell fusion in *Chlamydomonas*: analysis of wild-type gametes and nonfusing mutants. J. Cell Biol. **92:**378-386.

12. **Detmers PA, Goodenough UW, Condeelis J.** 1983. Elongation of the fertilization tubule in *Chlamydomonas*: new observations on the core microfilaments and the effect of transient intracellular signals on their structural integrity. J. Cell Biol. **97:**522–532.
13. **Detmers PA, Carboni JM, Condeelis J.** 1985. Localization of actin in *Chlamydomonas* using antiactin and NBD-phallacidin. Cell Motil. **5:**415–430.
14. **Nozaki H.** 1984. Newly found facets in the asexual and sexual reproduction of *Gonium pectorale* (Chlorophyta, Volvocales). Jpn. J. Phycol. **32:**130-133.
15. **Mogi Y, Hamaji T, Suzuki M, Ferris P, Mori T, Kabeya Y, Miyagishima S, Nozaki H.** 2012. Evidence for tubular mating structures induced in each mating type of heterothallic *Gonium pectorale* (Volvocales, Chlorophyta). J. Phycol. **48:**670-674.
16. **Ferris PJ, Goodenough UW.** 1997. Mating type in Chlamydomonas is specified by *mid,* the minus-dominance gene. Genetics **146:**859-869.
17. **Nozaki H, Mori T, Misumi O, Matsunaga S, Kuroiwa T.** 2006. Males evolved from the dominant isogametic mating type. Curr. Biol. **16:**R1018-R1020.
18. **Hamaji T, Ferris PJ, Coleman AW, Waffenschmidt S, Takahashi F, Nishii I, Nozaki H.** 2008. Identification of the minus-dominance gene ortholog in the mating-type locus of *Gonium pectorale*. Genetics **178:**283-294.
19. **Ferris P, Olson BJSC, De Hoff PL, Douglass S, Casero D, Prochnik S, Geng S, Rai R, Grimwood J, Schmutz J, Nishii I, Hamaji T, Nozaki H, Pellegrini M, Umen JG.** 2010. Evolution of an expanded sex-determining locus in *Volvox*. Science **328:**351-354.
20. **Hiraide R, Kawai-Toyooka H, Hamaji T, Matsuzaki R, Kawafune K, Abe J, Sekimoto H, Umen J, Nozaki H.** 2013. The evolution of male-female sexual dimorphism predates the gender-based divergence of the mating locus gene *MAT3/RB*. Mol. Biol. Evol. **30:**1038-1040.

21. **Hamaji T, Smith DR, Noguchi H, Toyoda A, Suzuki M, Kawai-Toyooka H, Fujiyama A, Nishii I, Marriage T, Olson BJSC, Nozaki H.** 2013. Mitochondrial and plastid genomes of the colonial green alga *Gonium pectorale* give insights into the origins of organelle DNA architecture within the Volvocales. PLoS ONE **8:**e57177. doi:10.1371/journal.pone.0057177.

22. **Yamada TK, Nakada T, Miyaji K, Nozaki H.** 2006. Morphology and molecular phylogeny of *Gonium multicoccum* (Volvocales, Chlorophyceae) newly found in Japan. J. Jpn. Bot. **81:**139-147.

23. **Tamura K, Peterson D, Peterson N, Stecher G, Nei M, Kumar S.** 2011. MEGA5: molecular evolutionary genetics analysis using maximum likelihood, evolutionary distance, and maximum parsimony methods. Mol. Biol. Evol. **28:**2731-2739.

24. **Thompson JD, Gibson TJ, Plewniak F, Jeanmougin F, Higgins DG.** 1997. The CLUSTAL_X windows interface: flexible strategies for multiple sequence alignment aided by quality analysis tools. Nucleic Acids Res. **25:**4876–4882.

25. **Stamatakis A, Hoover P, Rougemont J.** 2008. A rapid bootstrap algorithm for the RAxML web-servers. Syst. Biol. **75:**758–771.

26. **Guindon S, Dufayard JF, Lefort V, Anisimova M, Hordijk W, Gascuel O.** 2010. New algorithms and methods to estimate maximum-likelihood phylogenies: assessing the performance of PhyML 3.0. Syst. Biol. **59:**307–210.

27. **Arakaki Y, Kawai-Toyooka, Hamamura Y, Higashiyama T, Noga A, Hirono M, Olson BJSC, Nozaki H.** 2013. The simplest integrated multicellular organism unveiled. PLoS ONE 8:e81641. doi:10.1371/journal.pone.0081641.

28. **Liu Y, Misamore MJ, Snell WJ.** 2010. Membrane fusion triggers rapid degradation of two gamete- specific, fusion-essential proteins in a membrane block to polygamy in *Chlamydomonas.* Development **137:**1473-1481.

29. **Sprunck S, Rademacher S, Vogler F, Gheyselinck J, Grossniklaus U, Dresselhaus T.** 2012. Egg cell-secreted EC1 triggers sperm cell activation during double fertilization. Science **338:**1093-1097.

30. **Nozaki H, Ito M.** 1994. Phylogenetic relationships within the colonial Volvocales (Chlorophyta) inferred from cladistic analysis based on morphological data. J. Phycol. **30:**353–365.

31. **Nozaki H, Misawa K, Kajita T, Kato M, Nohara S, Watanabe MM.** 2000. Origin and evolution of the colonial Volvocales (Chlorophyceae) as inferred from multiple, chloroplast gene sequences. Mol. Phylog. Evol. **17:**256-268.

32. **Nozaki H**. 2003. Origin and evolution of the genera *Pleodorina* and *Volvox* (Volvocales). Biologia **58:**425-431.

33. **Herron MD, Hackett JD, Aylward FO, Michod RE.** 2009. Triassic origin and early radiation of multicellular volvocine algae. Proc. Natl. Acad. Sci. U. S. A. **106:**3254-3258.

34. **Martínez DE, Iñiguez AR, Percell KM, Willner JB, Signorovitch J, Campbell RD.** 2010. Phylogeny and biogeography of *Hydra* (Cnidaria: Hydridae) using mitochondrial and nuclear DNA sequences. Mol. Phylogenet. Evol. **57:**403-410.

FIG 1

Illustration of the advantages of *Gonium pectorale* for use in elucidating the mating-type specification of GCS1/HAP2. (A) Simplified diagram of phylogenetic relationships of selected genera in the volvocine lineage. The stepwise transition from isogamy to anisogamy/oogamy is considered to be associated with the evolution of multicellularity (31–33). The *minus*- and male-specific presence of the *minus*-dominance (*MID*) genes in isogamous (*Chlamydomonas reinhardtii* [16] and *G. pectorale* [18]), anisogamous (*Eudorina* sp. [20] and *Pleodorina starrii* [17]), and oogamous (*Volvox carteri* [19]) species are also indicated in the diagram. (B) Sexual reproduction and separately induced gamete activation in *G. pectorale*. Vegetative colonies of *plus* and *minus* strains differentiate as gametes by long-term cultivation and mixing of the sexes, inducing gamete activation that leads cell walls to shed and tubular mating structures (TMSs) to emerge. The activated gametes fuse to form a zygote that undergoes meiosis to produce genetically diverse progenies. Alternatively, gamete activation can be induced without mixing of the sexes, by treatment with db-cAMP and IBMX (15). (C–E) Differential-interference contrast image of a 16-celled vegetative colony of a *plus* strain (C), and phase-contrast images of separately activated gametes of *plus* (D) and *minus* (E) strains of *G. pectorale*. TMSs (filled arrowheads) emerge in activated gametes. Scale bars, 10 μm.

FIG 2

Identification of the *GCS1* ortholog in *Gonium pectorale*. (A) Structure of the *GpGCS1* gene. Solid and open boxes represent coding and non-coding exon sequences, respectively. Solid lines indicate introns. Polyadenylation sites and the positions of primers used for RT-PCR analysis are also indicated. (B) Alignment of deduced amino acid sequences of GCS1/HAP2

from *G. pectorale* (upper) and *C. reinhardtii* (lower). Identical and similar residues are shaded in black and gray, respectively. Signal sequences, HAP2-GCS1, and transmembrane domains are indicated by boxes. Asterisks within the HAP2-GCS1 domain represent invariant cysteine residues conserved among the GCS1/HAP2 homologs. Open triangles indicate putative N-glycosylation sites. The region corresponding to the antigen used to generate anti-GpGCS1 antibody is also marked.

FIG 3

Phylogeny of GCS1/HAP2 proteins from various eukaryotic lineages, including GpGCS1 identified in this study. Asterisks indicate species in which exclusive and/or functional GCS1 expression resides in the male or its homologous sex (5-8). Note that *Hydra magnipapillata* was synonymized with *H. vulgaris* (34). The tree was constructed using the RAxML (with WAG+I+4G model) method with a data matrix of 239 amino acid positions from the 29 operational taxonomic units. Left and right bootstrap values (≥ 50%) were obtained using the RAxML and PhyML (with LG+I+4G model) methods, respectively. Note that Streptophyta, Alveolata, Chlorophyta and Opisthokonta include land plants, malaria parasites, volvocine greens, and metazoans, respectively. The accession numbers of the sequences are as follows: AAY42350 (*Leishmania major* B), GCA_000004985.1 (jgi|Naegr1|50939|fgeneshHS_pg.scaffold_40000024, *Naegleria gruberi*), XP_843157 (*Leishmania major* A), XP_823296 (*Trypanosoma brucei*), XP_814894 (*Trypanosoma cruzi*), XP_005536505 (*Cyanidioschyzon merolae*), XP_002952883 *(V. carteri* 2), XP_002952884 (*V. carteri* 1), ABO29824 (*C. reinhardtii*), AB915401 (*G. pectorale*), EIE26501.1 (*Coccomyxa subellipsoidea*), XP_001431224 (*Paramecium tetraurelia* B), XP_001432430 (*Paramecium tetraurelia* A), XP_001030543 (*Tetrahymena thermophila*), XP_764209

(*Theileria parva*), XP_676900 (*Plasmodium berghei*), XP_725086 (*Plasmodium yoelii*), NP_700613 (*Plasmodium falciparum*), ESS30604 (*Toxoplasma gondii*), AAY51998 (*Arabidopsis thaliana*), BAE71142 (*Lilium longiflorum*), NP_001055054 (*Oryza sativa*), XP_643321 (*Dictyostelium discoideum*), ABN45755 (*Hydra vulgaris = H. magnipapillata*), XP_001628495 (*Nematostella vectensis*), XP_001746497 (*Monosiga brevicollis*), GCA_000002195.1(gnl|Amel_4.5|Group5.13 GL630243.1, *Apis mellifera*), XP_973371 (*Tribolium castaneum*), and BAE71144 (*Physarum polycephalum*).

FIG 4

Semi-quantitative RT-PCR of *GpGCS1* expression in strains K41 (mating-type *plus*) and K34 (mating-type *minus*). Polyadenylated mRNAs from vegetative cells, gametes, and activated gametes of *plus* and *minus* strains were isolated and subjected to semi-quantitative RT-PCR analysis. Expression levels were also examined at the indicated times after mixing *plus* and *minus* gametes. *GpMID* expression was examined to confirm gamete induction in the *minus* strain. The loading volume for each lane was normalized to the quantity of *EF-like* gene (internal control) product.

FIG 5

Immunoblotting analysis of GpGCS1 expression in strains K41 (mating-type *plus*) and K34 (mating-type *minus*). (A) Gamete-specific, *minus*-enhanced expression of GpGCS1. Total protein from each sample was subjected to SDS-PAGE, blotted, and probed with anti-GpGCS1 antibody. CBB-staining of a duplicate gel shows equal protein loading in each lane. (B) *Plus*-specific degradation of GpGCS1 in activated gametes. *Plus* or *minus* gametes from

the same culture were harvested before and after incubation with db-cAMP and IBMX for the indicated times, and subjected to immunoblotting analysis as in (A).

FIG 6

Immunofluorescence analysis of GpGCS1 localization in strains K41 (mating-type *plus*) and K34 (mating-type *minus*). (A) Unactivated *minus* and *plus* gametes were stained with anti-GpGCS1 antibody. The fluorescence images are maximum-intensity projections from confocal z-stacks. Images formed by merging the fluorescence and differential interference contrast (DIC) images are also shown. Asterisks and arrowheads indicate flagella and their roots, respectively. Scale bars, 5 μm. (B) *Minus* and *plus* gametes activated by db-cAMP and IBMX treatment were double-stained with anti-GpGCS1 and anti-actin antibodies. The merged and phase-contrast images are also shown. Arrowheads indicate the tips of the TMSs. Scale bars, 5 μm.

FIG 7

A model of the stepwise regulation of localization of GpGCS1 specifically to the *minus* TMS. The GpGCS1 protein level is enriched in *minus* gametes by transcriptional regulation (Step 1). Then, *minus*-specific transport to the primordial TMS site (Step 2) enables GpGCS1 to be present on the *minus* TMS upon activation. In contrast, GpGCS1 rapidly degrades in *plus* gametes (Step 3).

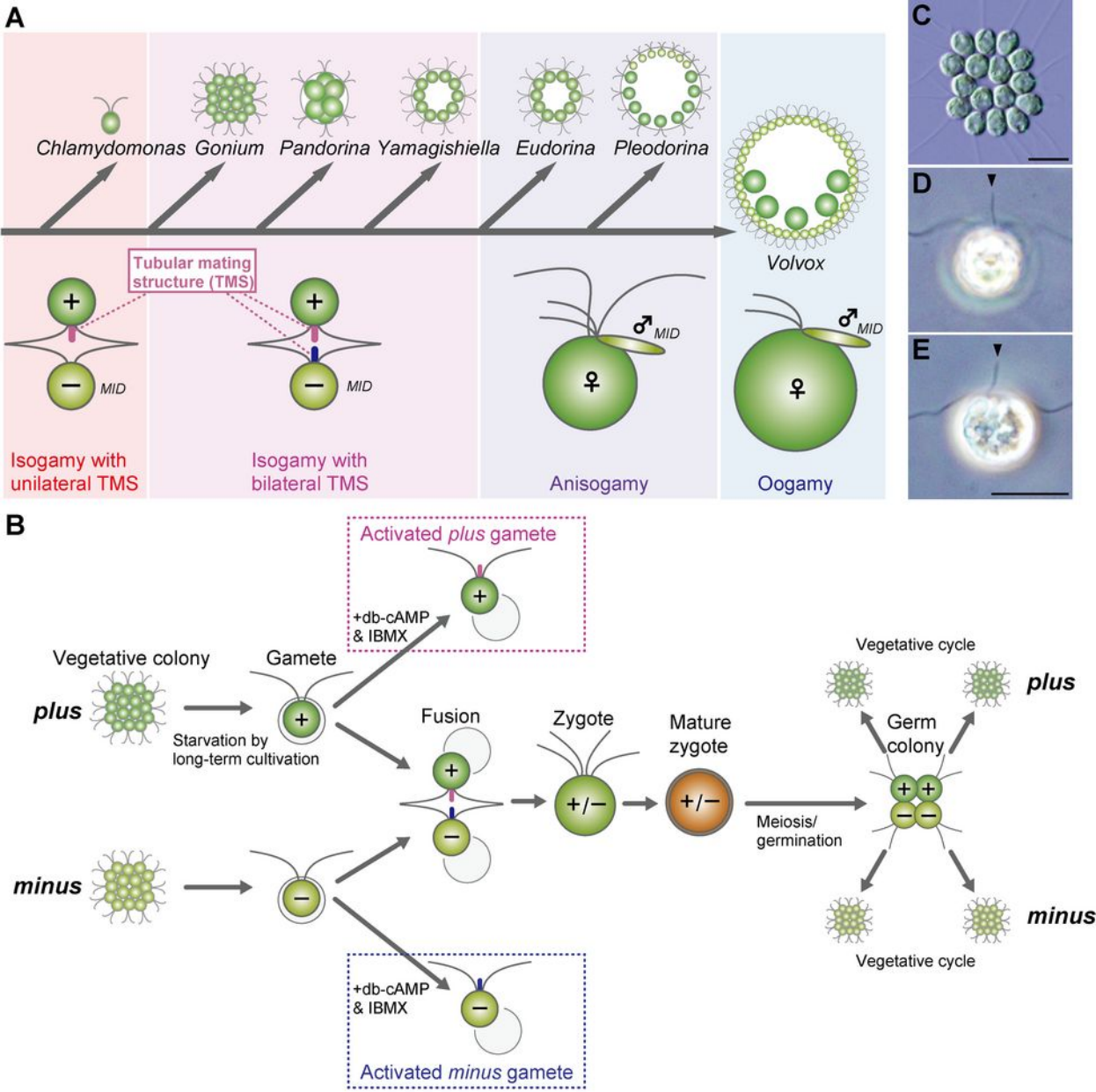
A
Chlamydomonas
Gonium
Pandorina
Yamagishiella
Eudorina
Pleodorina
Volvox
Tubular mating structure (TMS)
MID
MID
MID
MID
Isogamy with unilateral TMS
Isogamy with bilateral TMS
Anisogamy
Oogamy
C
D
E
B
Activated plus gamete
+db-cAMP & IBMX
Vegetative colony
Gamete
plus
Starvation by long-term cultivation
Fusion
Zygote
Mature zygote
+/−
+/−
Meiosis/ germination
Vegetative cycle
plus
Germ colony
minus
Vegetative cycle
minus
+db-cAMP & IBMX
Activated minus gamete

FIG 1

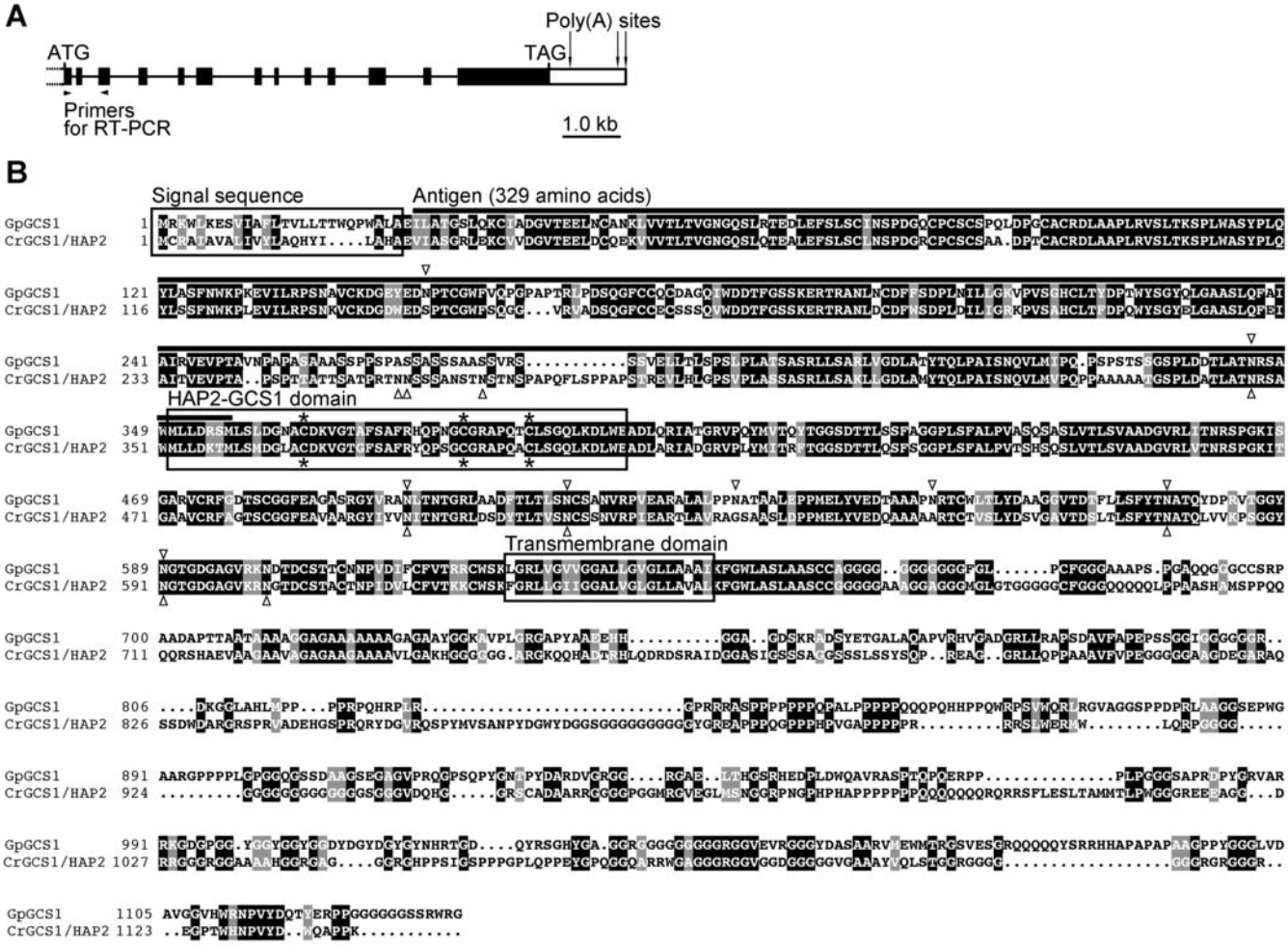
A
ATG
TAG
Poly(A) sites
Primers
for RT-PCR
1.0 kb
B
Signal sequence
Antigen (329 amino acids)
HAP2-GCS1 domain
Transmembrane domain
GpGCS1
CrGCS1/HAP2

FIG 2

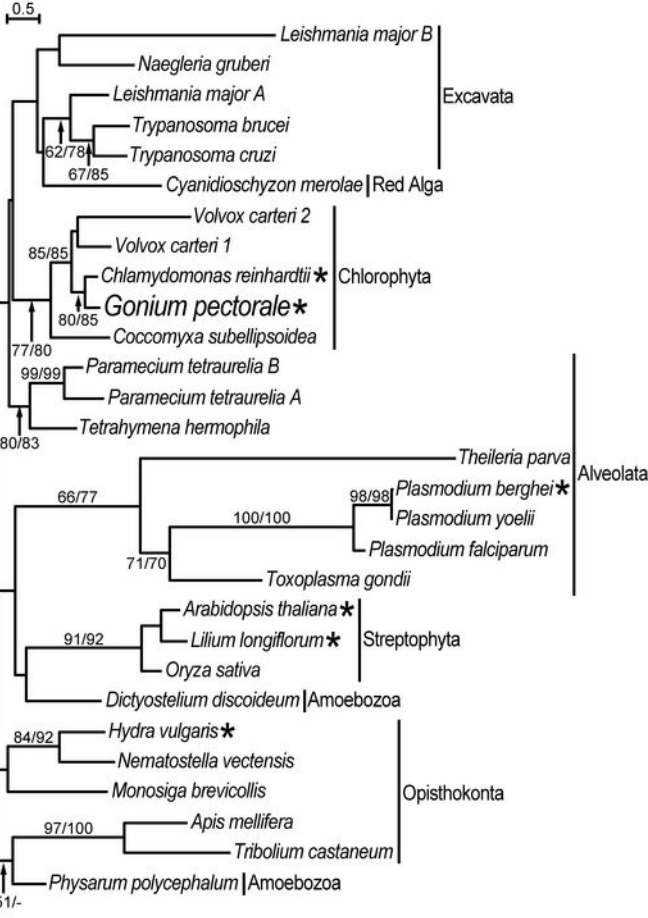
0.5
Leishmania major B
Naegleria gruberi
Leishmania major A
Trypanosoma brucei
Trypanosoma cruzi
Cyanidioschyzon merolae
Excavata
Red Alga
62/78
67/85
Volvox carteri 2
Volvox carteri 1
Chlamydomonas reinhardtii *
Gonium pectorale *
Coccomyxa subellipsoidea
Chlorophyta
85/85
80/85
77/80
Paramecium tetraurelia B
Paramecium tetraurelia A
Tetrahymena hermophila
99/99
80/83
Theileria parva
Plasmodium berghei *
Plasmodium yoelii
Plasmodium falciparum
Toxoplasma gondii
Alveolata
66/77
98/98
100/100
71/70
Arabidopsis thaliana *
Lilium longiflorum *
Oryza sativa
Streptophyta
91/92
Dictyostelium discoideum
Amoebozoa
Hydra vulgaris *
Nematostella vectensis
Monosiga brevicollis
Opisthokonta
84/92
Apis mellifera
Tribolium castaneum
97/100
Physarum polycephalum
Amoebozoa
51/-

FIG 3

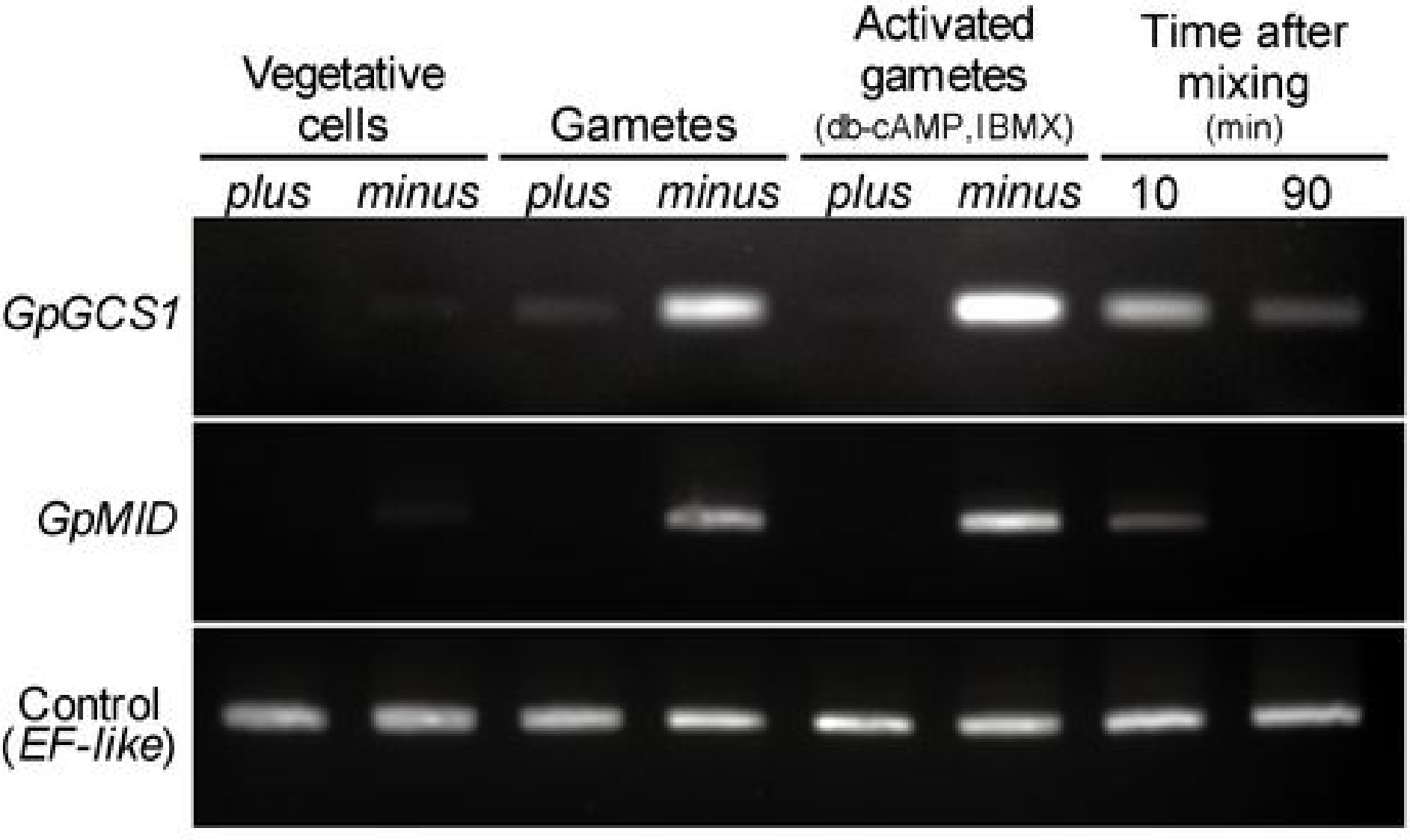
Vegetative cells
Gametes
Activated gametes (db-cAMP,IBMX)
Time after mixing (min)
plus
minus
plus
minus
plus
minus
10
90
GpGCS1
GpMID
Control (EF-like)

FIG 4

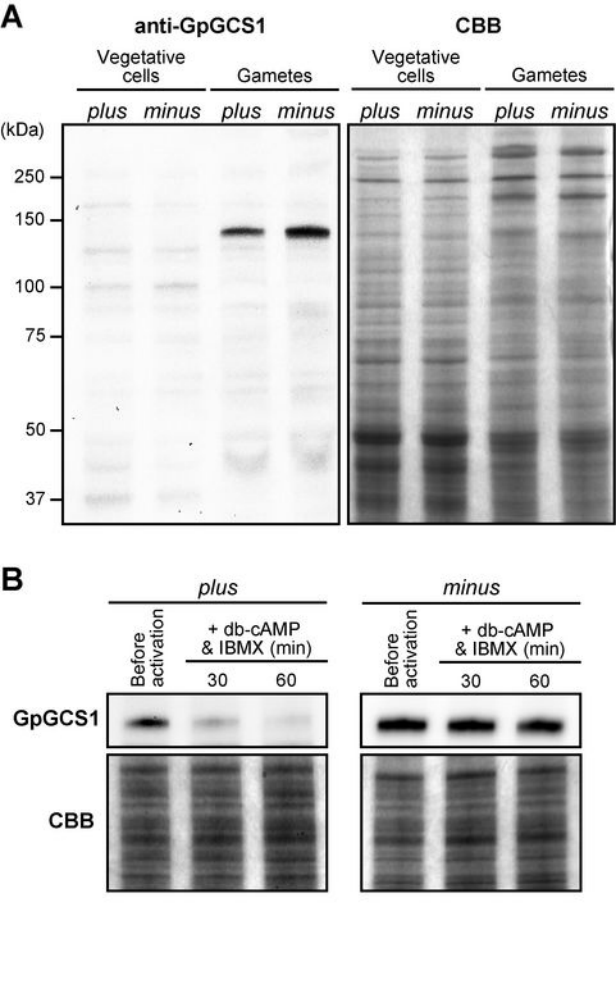
A
anti-GpGCS1
CBB
Vegetative cells
Gametes
plus
minus
(kDa)
250
150
100
75
50
37
B
plus
minus
Before activation
+ db-cAMP & IBMX (min)
30
60
GpGCS1
CBB

FIG 5

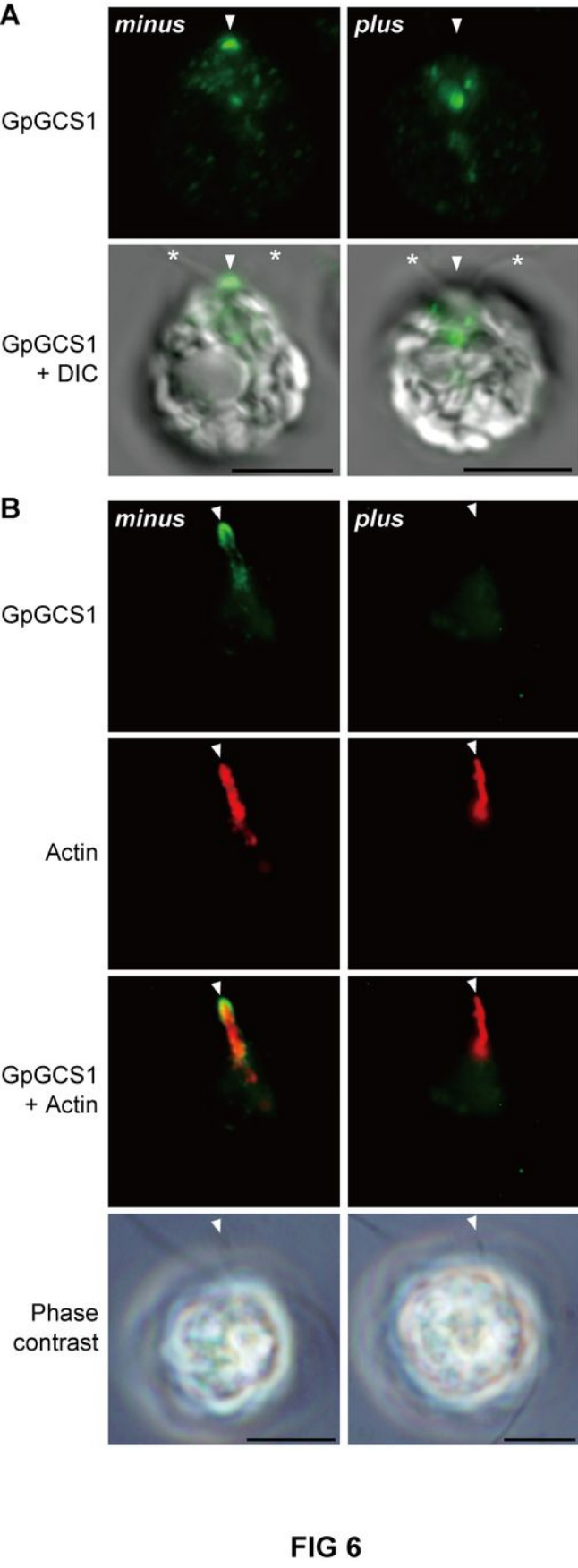
A
minus
plus
GpGCS1
GpGCS1
+ DIC
B
minus
plus
GpGCS1
Actin
GpGCS1
+ Actin
Phase
contrast

FIG 6

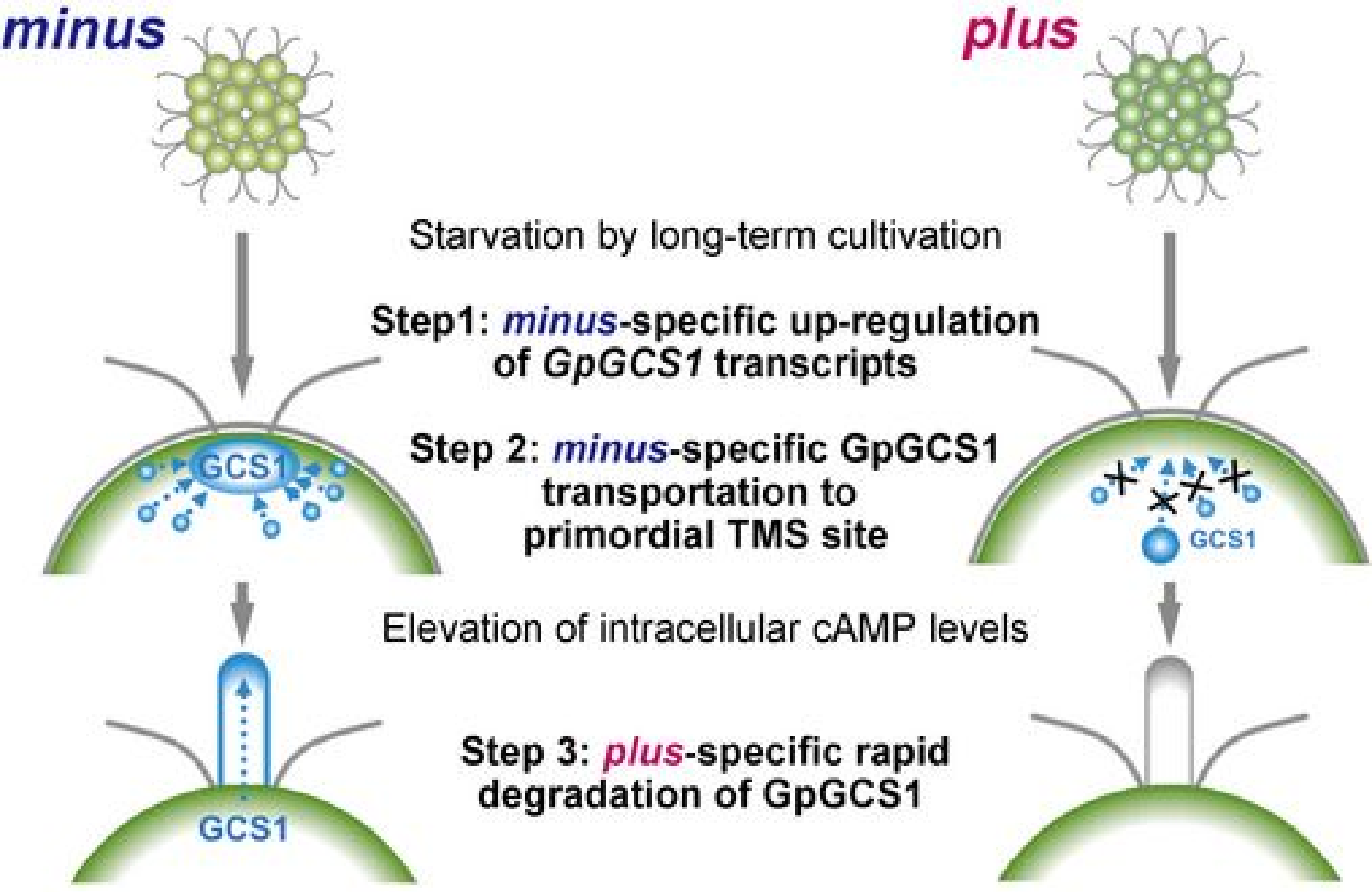
minus
plus
Starvation by long-term cultivation
Step1: minus-specific up-regulation of GpGCS1 transcripts
Step 2: minus-specific GpGCS1 transportation to primordial TMS site
GCS1
GCS1
Elevation of intracellular cAMP levels
Step 3: plus-specific rapid degradation of GpGCS1
GCS1

FIG 7